

Extension of a Charged Anisotropic United Atoms Model to Polycyclic Aromatic Compounds

Benoît Creton,* Theodorus de Bruin, Véronique Lachet, and Carlos Nieto-Draghi

Department of Thermodynamics and Molecular Modelling, IFP, 1-4 Avenue de Bois-Préau, 92852 Rueil-Malmaison, Cedex, France

Received: February 24, 2010; Revised Manuscript Received: April 2, 2010

A new potential model for polycyclic aromatic hydrocarbons has been developed on the basis of a charged anisotropic united atoms (AUA) potential with six AUA force centers and three electrostatic point charges per aromatic ring. Using quantum mechanical calculations, quadrupolar moments of several aromatic molecules were computed and a correlation has been observed that links the magnitude of the point charges with respect to the number of aromatic rings. The Lennard-Jones parameters of quaternary carbon atoms bridging two aromatic rings have been optimized with the minimization of a dimensionless error criterion incorporating various thermodynamic data of naphthalene. The new potential model, called ch-AUA, was then evaluated on its abilities to predict thermodynamic and transport properties for a series of polycyclic aromatic compounds in a wide range of temperatures. Although the relative errors with respect to the experimental density, vaporization enthalpy, and vapor pressure data are similar to those computed with the noncharged AUA potential, the new ch-AUA potential noticeably improves the prediction of the shear viscosities of polycyclic aromatic compounds. Comparisons between experimental viscosities of 1-methylnaphthalene at different pressures and those computed using the new ch-AUA and the noncharged AUA potentials show that the new potential improves the prediction of viscosities at high pressures.

1. Introduction

Following the world objectives regarding the global decrease of emissions of greenhouse gases, the automobile industry is focused on the problem of efficiency and consumption of engines. One way to reduce the emissions of those gases comes from the addition of 5–10% biodiesel in diesel blends. The development and the fine-tuning of flexi-fuel engines which are able to work with different types of blends require detailed information on thermophysical properties of those mixtures such as the density, vaporization enthalpy, and vapor pressure, as well as transport properties such as viscosity. Because of the high temperatures (up to 500 K) and pressures (250 MPa) that reign in engines under working conditions, the experimental measurements of those properties are expensive and difficult to realize. However, molecular modeling is nowadays capable of providing a reliable solution to overcome this obstacle.

As diesel blends are made up of a large number of different molecules (from linear alkanes to complex aromatic compounds),^{1,2} force fields thought to model the above-mentioned properties of such fuels must lead to accurate results for a reasonable computational cost. Among empirical force fields, all-atoms (AA) potentials, such as the optimized potential for liquid simulations (OPLS) potential,³ are probably the most realistic ones, but due to the computational resources required, they have not been envisaged for this study. Lately, a large effort has been devoted to the development of an anisotropic united atoms (AUA) model, in order to compute thermodynamic properties of diesel blend components such as linear and branched alkanes,⁴ alkenes,⁵ and aromatics molecules from benzene^{6,7} and alkylbenzenes⁸ to polycyclic aromatic hydrocarbons.⁹ Although all these developments improved the accuracy of the calculated

thermodynamic properties, AUA parameters appear less efficient when transport properties, such as viscosity, are considered. Recently, a new parametrization of the AUA potential for linear¹⁰ and branched¹¹ alkanes and alkenes was shown to yield a noticeable improvement for the prediction of viscosities for these molecules. For benzene¹² and alkylbenzenes,^{13,14} Nieto-Draghi et al. have developed a AUA model that explicitly takes into account the delocalization π -electrons of the aromatic ring using three point charges: $-q$ above and under the aromatic ring to embody the negative charge of the aromatic electron cloud, and $+2q$ charge localized at the center of the plane defined by the aromatic ring. Using this so-obtained ch-AUA potential model for monoaromatic compounds, both thermodynamic and transport properties are consistent with experimental data. In addition, in the perspective of simulations of diesel/biodiesel blends, the electrostatic interactions between aromatic rings and oxygenated molecules are thought to play an important role in the prediction of mixture properties which justifies the choice of an explicit account of the polarity of such molecules.

The purpose of the present article is to develop an extension of the ch-AUA potential to deal with polycyclic aromatic hydrocarbons (PAH). Here, we consider the reparameterization of the Lennard-Jones interactions involving the quaternary carbon connecting two aromatic rings. The electrostatic interactions are modeled using point charges per aromatic ring following the approach previously used for benzene. The charges are optimized on the basis of quadrupolar moment values obtained by quantum mechanical calculations and thermophysical experimental data. A general rule that links the magnitude of the electrostatic point charges with the number of aromatic rings in the molecule is then proposed. Using Monte Carlo (MC) and molecular dynamics (MD) simulations, the new ch-AUA potential is tested for several PAH, on its abilities to reproduce experimental thermodynamic and transport properties. Since our

* Corresponding author. E-mail: benoit.creton@ifp.fr.

objective is to predict the viscosity of compounds at conditions that reign in engines under working conditions, high-temperature and -pressure simulations are performed.

The paper is organized as follows. In section 2, we present the expressions used to compute the intermolecular potential energy and more generally the simulation method. In section 3, we detail the procedure employed for the optimization process and the so-obtained parameters. Section 4 is devoted to the evaluation of the new ch-AUA potential model on naphthalene, anthracene, and phenanthrene and results computed for other aromatic molecules. This paper ends with section 5, which gives the conclusions.

2. Simulation Methods

2.1. Intermolecular Potential Model. The effective dispersion–repulsion interactions between two atoms or united atom centers (i and j) belonging to different molecules are represented by the Lennard-Jones 6–12 equation (1).

$$U_{\text{LJ}} = 4 \sum_i \sum_{j>i} \varepsilon_{ij} \left[\left(\frac{\sigma_{ij}}{r_{ij}} \right)^{12} - \left(\frac{\sigma_{ij}}{r_{ij}} \right)^6 \right] \quad (1)$$

where σ_{ij} and ε_{ij} are the Lennard-Jones interaction parameters between sites i and j , and $r_{ij} \equiv \mathbf{r}_j - \mathbf{r}_i$ represents the separation distance between these two sites. Cross interactions between centers of force of different types are treated using standard Lorentz–Berthelot combining rules.

The electrostatic energy, U_{el} , is obtained by summing the pairwise Coulombic interactions between the partial charges belonging to different molecules.

$$U_{\text{el}} = \frac{1}{4\pi\epsilon_0} \sum_i \sum_{j>i} \frac{q_i q_j}{r_{ij}} \quad (2)$$

where q_i and q_j are the charges of different centers of interaction and ϵ_0 is the dielectric constant of vacuum. In both types of simulations (MD and MC), the Ewald summation technique is used to treat the long-range electrostatic interactions with seven vectors on each direction of the space and a scaling parameter $\alpha = 2[\pi/L] \text{ \AA}^{-1}$ in the direct space with a spherical cutoff equal to half the simulation box.

As is commonly assumed,^{15–18} the aromatic molecules are considered to be rigid. Consequently, no stretching, bending, or torsion energy is computed. In the case of an alkyl substituent on a ring, the α -carbon atom is assumed to lie within the aromatic ring plane with a bond angle value of 120° .^{19,20}

2.2. MD Simulations and Dynamic Properties. The aim of this work is to develop an extension of the charged AUA potential and test its abilities to reproduce, among other properties, the shear viscosity of pure compounds. The dynamic properties are computed using Newton,²¹ a molecular dynamics code developed for flexible and rigid molecules, where the velocity Verlet algorithm is used to integrate the equations of motion. In order to improve the statistics on the prediction of the viscosity, five MD runs, each starting with different initial conditions, are computed for all the studied systems. All simulation samples consist of 200 molecules. The molecules are initially placed in a cubic box using periodic boundary conditions, and the initial density is the parameter that differs between the five simulation boxes. A run is divided into two parts: the first one, having a length of 100 ps, is devoted to the equilibration of the system at the desired temperature and pressure through NPT rescaling using a weak coupling bath²² with long-range corrections²³ for pressure and energy. Unless specified otherwise, the second part, also called the production

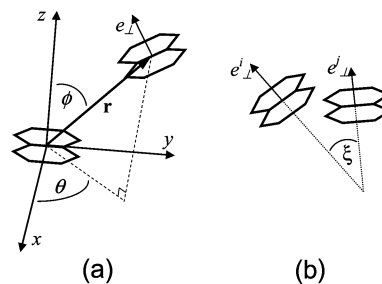


Figure 1. Local system of reference (a) and relative angle orientation ξ (b).

run, consists of a 8 ns length simulation for each system. The integration of equations of motion is performed with a time step of 2 fs. A Verlet nearest-neighbor list is also employed to improve the performance of the simulations. Finally, the reported calculated properties result from the average of the five independent runs.

To investigate the liquid equilibrium structure of the studied compounds, we have used the spatial distribution function (SDF), which yields information about the local structure of molecules

$$g(\mathbf{r}) = \frac{1}{\rho} \rho(\mathbf{r}) \quad (3)$$

where $g(\mathbf{r})$ is the SDF of a molecule of average number density ρ and \mathbf{r} is a three-dimensional position vector defined in polar coordinates. This function can be computed between different interaction sites a and b for molecular liquids (i.e., $g_{ab}(\mathbf{r})$), and the well-known radial distribution function (RDF) is defined as

$$g_{ab}(r) = \int g_{ab}(\mathbf{r}) d\Omega \quad (4)$$

where $\Omega \equiv (\theta, \phi)$ is the solid angle in the molecular-fixed frame of reference. A local system of coordinates is placed at the geometric center of each molecule with one of the axes (z -axis) pointing in the perpendicular direction of the plane of the molecule and another (x -axis) pointing in the direction of the longest side of the molecule (see the Figure 1 for more details). As in previous works,^{12,13} the relative orientation between molecules is defined using unitary vectors \mathbf{e}_i^\perp and \mathbf{e}_j^\perp pointing in the perpendicular direction of the plane of molecules i and j , respectively (Figure 1a). A relative orientational SDF can be constructed by projecting the function

$$\text{orientation} = \cos(\xi) - 0.5 \quad (5)$$

on the isodensity surface probability, where the angle ξ is defined as presented in Figure 1b. In eq 5, the shifting value of 0.5 was chosen only to set values in the range -0.5 to 0.5 as ξ is defined between 0 and $\pi/2$.

The shear viscosity can be calculated either in the isobaric–isothermal ensemble (NPT) or in the canonical ensemble (NVT). As described in previous works,^{10–13} the Einstein relation was employed to calculate the shear viscosity of the systems of interest. The viscosity of the system is given by the expression

$$\eta = \frac{1}{20 k_B T} \lim_{t \rightarrow \infty} \frac{d}{dt} \left[\sum_{\alpha} \langle \Delta \mathbf{P}_{\alpha\alpha}(t)^2 \rangle + 2 \sum_{\alpha > \beta} \langle \Delta \mathbf{P}_{\alpha\beta}(t)^2 \rangle \right] \quad (6)$$

where α and β run over the three Cartesian coordinates, k_B is the Boltzmann constant, V is the volume, T is the temperature,

and $\Delta\mathbf{P}_{\alpha\beta}$ denotes the displacement of the elements of the pressure tensor $\mathbf{P}_{\alpha\beta}$.

2.3. MC Simulations and Thermodynamic Properties.

Thermodynamic properties were computed using the GIBBS Monte Carlo code.²⁴ Periodic boundary conditions were applied with the minimum image convention.²⁵ Dispersion–repulsion interactions were evaluated with a spherical cutoff radius equal to half the size of the cubic simulation box, associated with standard long-range corrections for the total energy and pressure.

Phase Equilibria. The Gibbs ensemble Monte Carlo method²⁶ was used to compute the liquid–vapor equilibria of aromatic polycyclic compounds. The MC simulations were carried out with a total of 170 molecules. The implemented MC moves are translations, rigid body rotations, transfers,²⁷ and volume changes. For transfers of rigid molecules we have used a two-step statistical bias involving the selection of a suitable location for the center of mass in the first step and the test of several orientations for the second step.²⁸ The simulations were initialized with 100 molecules representing the liquid simulation box, and the 70 remaining ones were chosen to represent the vapor state. MC simulations were split into two parts: the first can be seen as an equilibration of the system, and the selected probabilities for the Monte Carlo moves were set to 0.4975 for translations, 0.4975 for rotations, and 0.005 for volume changes. Typically, between 3×10^7 and 1×10^8 configurations were generated during the second part, where the Monte Carlo probability moves were set to 0.2725 for translations, 0.2725 for rotations, 0.4500 for transfers, and 0.005 for volume changes.

The molar enthalpy of vaporization is computed as the difference between the average molar enthalpies of the liquid and of the vapor simulation boxes. The statistical uncertainty on this property is typically 1–2%. The average liquid density is generally determined with a statistical uncertainty of 0.5–1%, but higher values are found at near-critical temperatures as a result of larger fluctuations. Critical properties were determined from the regression of scaling laws on the coexistence densities.²⁴

Thermodynamic Properties of the Liquid Below the Boiling Point. To overcome problems of transfers when the Gibbs ensemble is used below the normal boiling point, simulations were performed in the isobaric–isothermal ensemble (NPT) for these temperatures. Simulations were performed on systems of 150 molecules. Between 3×10^7 and 1×10^8 configurations were generated to obtain liquid properties with selected probabilities for the Monte Carlo moves set to 0.4960 for translations, 0.4960 for rotations, and 0.008 for volume changes.

The molar vaporization enthalpy, ΔH_{vap} has been calculated with the equation

$$\Delta H_{\text{vap}} = -\langle E_{\text{liq}} \rangle + RT \quad (7)$$

where T is the temperature, R is the ideal gas constant, and $\langle E_{\text{liq}} \rangle$ denotes the average molar intermolecular potential energy in the simulation. This relationship assumes that the vapor phase behaves as an ideal gas and that the molar volume of the liquid is negligible compared to the vapor volume. These assumptions are acceptable below the normal boiling point, because of the low density of the saturated vapor. As liquid properties do not significantly vary between the experimental vapor pressure and the modeled vapor pressure, the pressure was set to the experimental value for the NPT simulations.

For the simulations carried out with the NPT ensemble, the saturated vapor pressures, P_{sat} , are computed using the thermo-

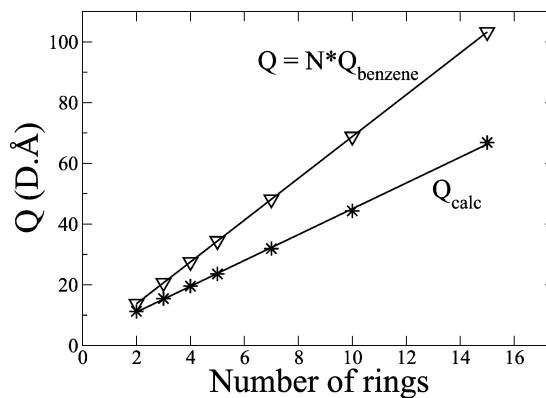


Figure 2. Evolution of the quadrupolar moment value with the number of aromatic rings in the molecule obtained by quantum calculations (stars) or by considering Q as the product of the benzene quadrupolar moment by the number of rings (triangles).

dynamic integration of the Clapeyron equation with a second-order numerical integration algorithm²⁹

$$\ln(P_{\text{sat}}(T_{n+2k})) = \ln(P_{\text{sat}}(T_n)) -$$

$$\frac{2}{R} \Delta(1/T) \sum_{i=1}^k \Delta H_{\text{vap}}(T_{n+2i-1}) \quad (8)$$

where $\Delta(1/T) = 1/T_i - 1/T_{i+1}$ is a constant. This relationship requires the two highest temperatures to be computed with the Gibbs ensemble.

2.4. Quantum Mechanical Calculations. The quantum mechanical calculations were performed at the B3LYP/6-311+G(d,p) level of theory using the Jaguar program (version 7.0; Schrödinger LLC)³⁰ with the highest symmetry constraint of the molecule (i.e., D_{6h} for benzene, D_{2h} for naphthalene, ...). Default convergence (10^{-6} hartree) for the electronic (self-consistent field) criterion and the default geometry convergence criteria have been applied. The atomic charges were calculated for the optimized structure from the electrostatic potential using the CHELPG scheme as implemented in Jaguar.^{31–33}

3. Optimization of the Potential Parameters

In previous works,^{12–14} properties of monocyclic aromatic compounds were successfully simulated using a AUA charged potential. A positive partial charge was placed at the center of the ring, and two negative partial charges representing the π -electron clouds were placed on each side of the ring, at a distance of 0.4 Å from the positive partial charge and perpendicularly to the plane of the aromatic ring. For instance, to mimic the quadrupolar moment of benzene molecule, the central and the two out-of-plane charges were set to $8.130e$ and $-4.065e$ leading to a quadrupolar moment ($-20.8 \times 10^{-40} \text{ C} \cdot \text{m}^2$) slightly lower than experimental values (-28.3×10^{-40} and $-33.3 \times 10^{-40} \text{ C} \cdot \text{m}^2$ for the works of Dennis et al.³⁴ and Vbrancich et al.,^{35,36} respectively). For a molecule with a methyl group bonded to an aromatic carbon, the partial positive charge lying in the plane of the ring was displaced by $\delta\mu$ from the center of the ring in order to mimic the dipole moment of the molecule.

To extend this approach to other polycyclic aromatic hydrocarbons, we have computed the quadrupolar moment (Q_N)_{DFT} of different molecules using DFT quantum mechanical calculations (values are available in the Supporting Information). As shown in Figure 2, the quadrupolar moment of an N -order PAH cannot be considered as the product of N times the quadrupolar moment of benzene, as this last assumption overestimates the calculated value. We have therefore decided to refer to the ab

TABLE 1: Potential Parameters Used in This Work^{13,14} and Value of the Positive Central Point Charge for N (Number of Aromatic Rings) Equal to 2, 3, and 4

group	σ (Å)	ϵ (K)	δ_{AUA} (Å)	N	$+2q$ (el)
CH aro	3.361	75.60	0.315	2	6.223
C aro ^a	3.361	43.00	0.000	3	5.759
C aro ($-\text{CH}_3$)	3.361	35.43	0.000	4	5.478
CH_3	3.607	120.15	0.216		

^a Parameters optimized in this work.**TABLE 2: Thermodynamic Data and Simulation Conditions Used for the Optimization of the ch-AUA Potential Parameters Using Naphthalene as Reference Molecule**

properties	simulation—ensemble	T (K)	simulated values	exptl data	AAD (%)
P_{sat} (kPa)			332.6 ± 14.5	329.9	0.81
ΔH_{vap} (kJ·mol ⁻¹)	MC—Gibbs	550	41.0 ± 14.3	38.3	7.10
ρ (kg·m ⁻³)			819.1 ± 2.2	803.4	1.95
η (mPa·s)	MD—NPT	400	0.572 ± 0.060	0.579	1.24

initio quadrupolar moment in order to estimate the set of charges of each molecule as a function of the number of aromatic rings N .

It appeared that the Lennard-Jones parameters of quaternary carbon atoms optimized by Nieto-Draghi et al. for alkylbenzenes,^{13,14} when applied to quaternary (bridging) aromatic carbon atoms, do not well reproduce liquid–vapor thermodynamic data. We have therefore reoptimized these parameters using the following dimensionless error criterion:²⁹

$$F = \sum_{i=1}^{\text{nbp}} \frac{(X_i^{\text{mod}} - X_i^{\text{exp}})^2}{S_i^2} \quad (9)$$

where i runs over properties (see below), X_i^{exp} and X_i^{mod} are the reference experimental measurement and the computed property, respectively, and S_i is the estimated statistical uncertainty on X_i^{mod} calculated by the block averaging technique.²⁵ F is considered to be a function of the parameters y_k to be optimized. The minimization of F with respect to all y_k is made by approximating the function by its first-order Taylor expansion. For this purpose, the partial derivatives $\partial X_i^{\text{mod}} / \partial y_k$ are evaluated by finite differences with the initial set of parameters.

The optimization procedure has been performed at 400 and 550 K using naphthalene as a reference molecule, and experimental data were taken from the DIPPR database.³⁷ The bond lengths and the CH group parameters (σ , ϵ , δ_{AUA}) previously developed for benzene¹² and alkylbenzenes^{13,14} were used without modification. In order to ensure a planar geometry of the polycyclic aromatic hydrocarbons, the σ -parameter of the quaternary carbon was fixed during the optimization procedure at the same value as that of σ -parameter for CH aromatic group. We have used the following iterative procedure:

1. The ϵ -parameter of the quaternary carbon previously developed for alkylbenzenes were used as an initial guess. Positions and the arrangement of the point charges are fixed on each aromatic ring, as described at the beginning of this section. Their magnitude was initially set to reproduce the quadrupolar moment obtained from the ab initio calculations. For naphthalene, liquid–vapor thermodynamic data were then computed to evaluate the error function (9) with $i = P_{\text{sat}}$, ΔH_{vap} , and ρ_{liq} leading to a new ϵ -parameter for the quaternary carbon.

2. The shear viscosity (η) is then computed and the error function (9) with $i = \eta$ is evaluated to obtain a new set of charges, i.e., quadrupolar moment.

3. Thermodynamics properties were then computed and compared with experimental data. If the desired precision is acquired,

the procedure is stopped; otherwise a new ϵ -parameter for the quaternary carbon is upgraded and one goes back to step number 2.

The optimized set of parameters is shown in Table 1, and the computed properties together with the corresponding absolute average deviations (AAD) are gathered in Table 2.

Following this procedure, we have optimized the parameters for naphthalene. In order to extrapolate our potential to polycyclic compounds having more than two rings, we have made the following assumptions: (i) the optimized Lennard-Jones parameters are transferable and (ii) the magnitude of the point charges is the only parameter that needs to be adapted to represent the appropriate electrostatic interactions. Consequently, we have used an empirical approach taking into account the ratio between the quadrupolar moment obtained by the optimized empirical potential of naphthalene ($Q_{N=2}^{\text{ch-AUA}}\text{opt}$) and the DFT one ($Q_{N=2}\text{DFT}$) as follows:

$$\frac{(Q_{N=2}^{\text{ch-AUA}})_{\text{opt}}}{(Q_{N=2})_{\text{DFT}}} = 0.848 \approx \frac{Q_N^{\text{ch-AUA}}}{(Q_N)_{\text{DFT}}} \quad (10)$$

where $Q_N^{\text{ch-AUA}}$ is the predicted quadrupolar moment of an N -order polycyclic aromatic compound represented by the ch-AUA potential. Finally, the value of the positive central point charge ($+2q$) in each ring of an N -order aromatic polycyclic molecule can be obtained according to eq 11.

$$+2q = 0.848 \frac{(Q_{N=2})_{\text{DFT}}}{N \delta q^2} \quad (11)$$

$\delta q = 0.4$ Å is the distance between the positive charge located at the center of each aromatic ring and the two negative charges

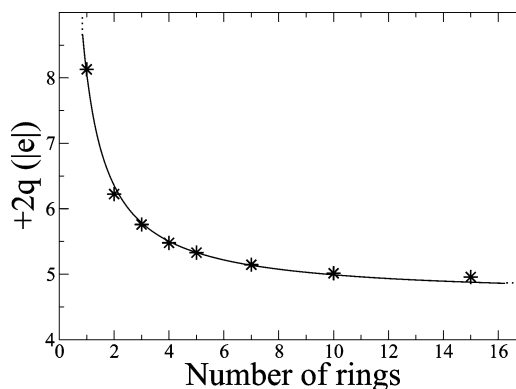
**Figure 3.** Variation of the point charge intensity with the number of aromatic rings in the molecule.

TABLE 3: Comparison between Equilibrium Properties of Naphthalene Obtained by Simulations with the Proposed ch-AUA Potential and Experimental Data from the DIPPR Database³⁷

<i>T</i> (K)	stat ensemble	density of liquid (kg•m ⁻³)			ΔH_{vap} (kJ•mol ⁻¹)			<i>P</i> _{sat} (kPa)		
		simul	expt	% error	simul	expt	% error	simul	expt	% error
352.0	NPT	997.4	979.4	1.8	53.8	52.8	2.0	0.7	0.9	-18.9
374.5	NPT	977.9	961.7	1.7	52.5	51.4	2.1	2.3	2.6	-13.0
400.0	NPT	957.6	941.1	1.8	51.1	49.7	2.8	6.4	7.2	-11.0
429.3	NPT	932.8	916.9	1.7	49.4	47.7	3.6	18.5	19.4	-4.7
463.0	Gibbs	903.9	887.3	1.9	47.2	45.3	4.1	48.6	51.3	-5.2
502.9	Gibbs	865.7	850.5	1.8	44.5	42.2	5.4	127.9	131.7	-2.9
550.0	Gibbs	819.1	803.3	2.0	41.0	38.3	7.1	332.6	326.4	1.9
606.9	Gibbs	755.9	738.8	2.3	36.0	32.7	10.0	845.0	789.4	7.0
676.9	Gibbs	654.7	637.8	2.6	27.3	23.8	14.8	2104.9	1896.8	11.0
AAD				2.0			5.7			8.4

TABLE 4: Comparison between Equilibrium Properties of Anthracene Obtained by Simulations with the Proposed ch-AUA Potential and Experimental Data from the DIPPR Database³⁷

<i>T</i> (K)	stat ensemble	density of liquid (kg•m ⁻³)			ΔH_{vap} (kJ•mol ⁻¹)			<i>P</i> _{sat} (kPa)		
		simul	expt	% error	simul	expt	% error	simul	expt	% error
480.5	NPT	1014.5	979.4	3.6	70.5	62.1	13.6	3.0	3.7	-19.2
518.8	NPT	985.5	949.0	3.8	67.6	60.3	12.2	9.4	11.6	-19.1
561.4	NPT	952.8	913.0	4.4	64.6	58.1	11.1	34.7	33.9	2.6
613.0	Gibbs	907.0	866.5	4.7	59.6	55.2	8.0	95.8	98.2	-2.4
675.1	Gibbs	815.2	805.3	1.2	53.8	51.1	5.4	300.2	274.6	9.3
AAD				3.5			10.0			10.5

TABLE 5: Comparison between Equilibrium Properties of Phenanthrene Obtained by Simulations with the Proposed ch-AUA Potential and Experimental Data from the DIPPR Database³⁷

<i>T</i> (K)	stat ensemble	density of liquid (kg•m ⁻³)			ΔH_{vap} (kJ•mol ⁻¹)			<i>P</i> _{sat} (kPa)		
		simul	expt	% error	simul	expt	% error	simul	expt	% error
373.0	NPT	1094.0	1066.4	2.6	75.6	69.3	9.1	0.0	0.0	-40.6
395.1	NPT	1080.0	1052.1	2.7	74.3	68.3	8.8	0.1	0.1	-36.5
419.9	NPT	1058.9	1035.7	2.2	72.5	67.1	8.0	0.3	0.4	-27.4
448.2	NPT	1039.7	1016.5	2.3	70.6	65.6	7.6	0.9	1.2	-24.5
480.5	NPT	1015.8	993.8	2.2	68.5	63.9	7.2	3.4	3.9	-13.9
517.8	NPT	989.0	966.4	2.3	66.1	61.8	7.0	10.9	12.2	-10.6
561.4	NPT	957.7	932.6	2.7	63.5	59.1	7.4	36.5	36.9	-1.1
613.0	Gibbs	914.0	889.4	2.8	58.8	55.7	5.6	107.8	107.2	0.6
675.1	Gibbs	857.2	831.1	3.1	53.3	50.7	5.1	304.4	300.8	1.2
AAD				2.5			7.3			17.4

located on each side of the ring. The variations of the magnitude of the positive central charge with the number *N* of aromatic rings can be seen in Figure 3.

4. Simulation Results

4.1. Thermodynamic Properties. MC simulations using the new parameters were performed at several temperatures different from those employed during the optimization procedure, to compute the thermodynamic properties of naphthalene. The results were compared to experimental data³⁷ and to results previously obtained with the noncharged AUA parameters.⁹ Furthermore, the thermodynamic properties of anthracene and phenanthrene obtained using the new ch-AUA potential were compared to experimental data and also to the results obtained with the noncharged AUA potential. Experimental data and results of our simulations are summarized in Tables 3–5 and illustrated in Figures 4–6. A recently published article deals with the parametrization of a force field for naphthalene, anthracene, and phenanthrene; our results are hereafter compared to data presented in this work.³⁸

Table 3 shows that, for naphthalene, the simulated values of the density, vaporization enthalpy, and vapor pressure are in good agreement with the experimental data. The new ch-AUA potential shows absolute average deviations (AAD) of 2.0, 5.7,

and 8.4 for the density, vaporization enthalpy, and vapor pressure (see Table 3), respectively. Ahunbay et al. report for the same properties deviations of 1.8, 2.0, and 15.5.⁹ Vapor pressure values computed by Desgrange et al. show with respect to experimental data an AAD of 7.8, which is in line with the

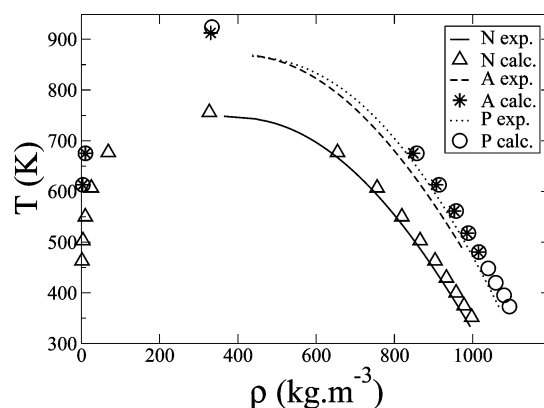


Figure 4. Comparison of densities of naphthalene (N), anthracene (A), and phenanthrene (P) computed with the new ch-AUA potential (calc.) with the correlation of experimental data (exp.) provided by the DIPPR database.³⁷ Critical coordinates are estimated using scaling law.

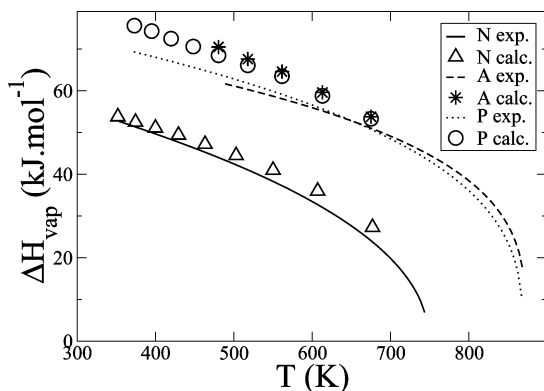


Figure 5. Comparison of vaporization enthalpies of naphthalene (N), anthracene (A), and phenanthrene (P) computed with the new ch-AUA potential (calc.) with the correlation of experimental data (exp.) provided by the DIPPR database.³⁷

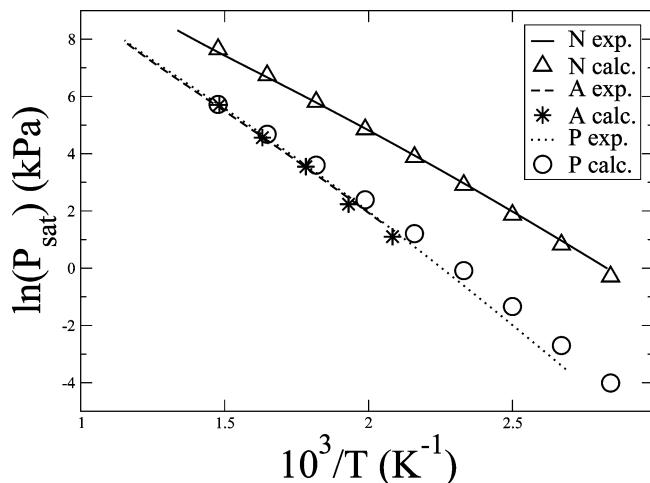


Figure 6. Comparison of vapor pressures of naphthalene (N), anthracene (A), and phenanthrene (P) computed with the new ch-AUA potential (calc.) with the correlation of experimental data (exp.) provided by the DIPPR database.³⁷

prediction of the ch-AUA potential. In addition, values calculated using ch-AUA lead to a normal boiling point of 490 K, which is in good agreement with the experimental value of 491 K.³⁷ Experimental critical density and temperature are 315 kg·m⁻³ and 748 K, respectively.³⁷ Our model returns an estimated critical density of 327 kg·m⁻³ and a critical temperature of 756 K, whereas the noncharged AUA potential leads to a critical density of 331 kg·m⁻³ and a critical temperature of 734 K,⁹ and Desgranges et al. report a critical density of 330 kg·m⁻³ and a critical temperature of 775 K.³⁸

Results of the simulated thermodynamic properties of anthracene are presented in Table 4, showing a good agreement with respect to experimental data. The AAD values obtained with the noncharged AUA potential are 3.3, 5.3, and 16.1 for the density, vaporization enthalpy, and vapor pressure, respectively.⁹ Although the ch-AUA potential improves the results of the vapor pressure, it deteriorates those of the vaporization enthalpy. In the case of the phenanthrene, results with the noncharged AUA potential show absolute average deviations of 4.1, 7.6, and 13.4 for the density, vaporization enthalpy, and vapor pressure, respectively.⁹ While both potentials lead to the same deviation with respect to experimental vaporization enthalpy, the ch-AUA exhibits a better agreement with respect to the experimental densities. Simulations using the ch-AUA potential yield normal boiling temperatures of 613 and 603 K

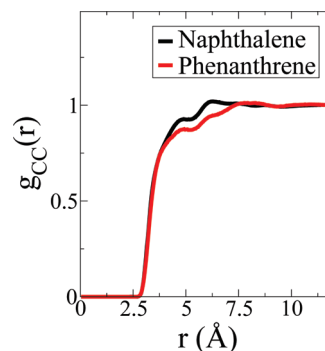


Figure 7. Radial distribution function (RDF) between carbon atoms obtained by the use of the new ch-AUA model and computed at 400 K and 0.1 MPa for naphthalene and phenanthrene.

for anthracene and phenanthrene, respectively, which are in good agreement with experimental data of 615 and 610 K, respectively.³⁷ For anthracene, experimental critical density and temperature are 322 kg·m⁻³ and 873 K, respectively.³⁷ Our model leads to a critical density of 330 kg·m⁻³ and a critical temperature of 913 K. In the case of phenanthrene, the DIPPR returns critical density and temperature of 322 kg·m⁻³ and 869 K, respectively.³⁷ Our model leads to a critical density of 334 kg·m⁻³ and a critical temperature of 924 K. The predicted critical properties are nearly similar to those computed by Desgranges et al. (for anthracene, $\rho_c = 338$ kg·m⁻³ and $T_c = 921$ K; for phenanthrene, $\rho_c = 343$ kg·m⁻³ and $T_c = 923$ K).³⁸ Compared to the noncharged AUA potential,⁹ our model slightly deteriorates the prediction of the critical temperature for these two compounds. Anthracene and phenanthrene have very similar thermodynamic properties. The differences between the vapor pressure and the vaporization enthalpies of these two compounds are lower than the simulation uncertainties on these properties. Therefore, we do not expect our potential to account for these differences.

If we only take into account the accuracy of the thermodynamic properties, we can observe that both potentials (AUA and ch-AUA) show similar AAD with respect to experimental data. As we will see hereafter, when transport properties are also considered, the charged model is considerably more accurate.

4.2. Structural Properties of Liquids. The liquid structures of naphthalene and phenanthrene represented by the carbon-carbon RDF computed with the ch-AUA model at 400 K and 0.1 MPa are presented in Figure 7. The liquid structures for both molecules are very similar and show an almost flat distribution. However, it is interesting to notice that the shoulder found for both fluids between 4 and 5 Å is also observed in monocyclic aromatics.^{12,13} This signature is characteristic of the AUA intermolecular potential, and it was previously reported in liquid benzene.¹² A small peak around 5.25 Å is only observed for naphthalene, whereas the RDF of phenanthrene increases smoothly to reach the bulk fluid structure. The presence of a small peak indicates a slightly higher localization in the first coordination shell in the case of naphthalene, with respect to phenanthrene. Unfortunately, we did not find any experimental data to compare our results with. In order to expand the analysis of the radial distribution functions (RDFs), we have also computed spatial distribution functions (SDFs), which have the advantage of showing details of the structures of fluids that are embedded in the angular averaged RDFs. A series of centers of mass to centers of mass SDFs using the ch-AUA model are presented in Figures 8 and 9 for naphthalene and phenanthrene, respectively. In both cases we represent the three-dimensional

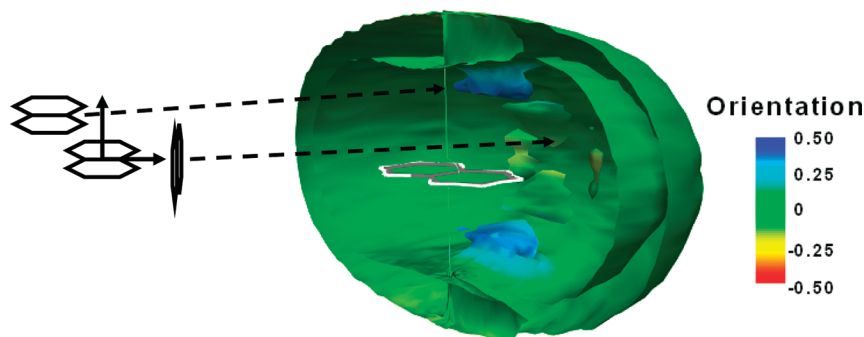


Figure 8. Center of mass to center of mass spatial distribution function (SDF) of naphthalene computed with the new ch-AUA model at $g(r, \theta, \varphi) = 0.7$ isodensity probability surface at 400 K and 0.1 MPa. The molecules inside the isodensity probability surface are placed as a guide to understand the SDF and do not represent the geometry of the ch-AUA model.

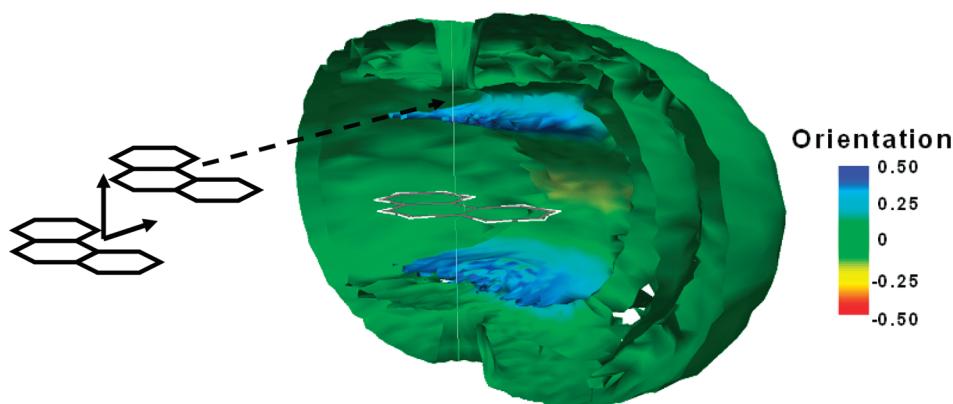


Figure 9. Center of mass to center of mass spatial distribution function (SDF) of phenanthrene computed with the new ch-AUA model at $g(r, \theta, \varphi) = 0.7$ isodensity probability surface at 400 K and 0.1 MPa. The molecules inside the isodensity probability surface are placed as a guide to understand the SDF and do not represent the geometry of the ch-AUA model.

isodensity probability surface for $g_{\text{cm}}(r, \Omega) = 0.7$ at 400 K and 0.1 MPa. Integration of these $g_{\text{cm}}(r, \Omega)$ functions over the solid angle Ω produces the RDFs presented in Figure 7. SDFs are indirectly accessible via neutron diffraction experiments through the empirical potential structure refinement (EPSR) method.^{39,40} Unfortunately, to the best of our knowledge, there are no experimental SDFs available for liquid polycyclic aromatics and only few simulation studies have been reported for aromatic compounds.^{12,13,41}

In Figure 8 we can observe the SDF describing the spatial localization of naphthalene molecules presenting different relative orientations of the vectors normal to the plane of the molecule as described in eq 5. Considering the magnitude of the projected functions, we observe that only at short distances the first neighboring molecule is arranged in a parallel conformation with respect to the reference one, but a slightly shifted conformation is shown in Figure 8 (see zones with positive values close to 0.5). We find a small probability of molecules placed with perpendicular orientation (T-shape form), and this probability is practically zero in the first solvation shell.

This arrangement of molecules is slightly different for phenanthrene as revealed by the SDF depicted in Figure 9. In this case, positive values of the SDF for parallel orientations are more important, but less localized than in the case of naphthalene. This observation is also coherent with the structure of the molecule itself, which presents three nonaligned aromatic rings allowing molecules to be arranged in sheet form in the first solvation shell.

4.3. Shear Viscosity. The shear viscosities computed for naphthalene, anthracene, and phenanthrene with the noncharged

AUA and the new ch-AUA potentials are gathered in Table 6, where they are compared to experimental data. These simulations were performed at temperatures higher than the experimental melting points: 353, 489, and 372 K for naphthalene, anthracene, and phenanthrene, respectively.³⁷

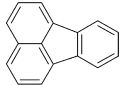
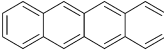
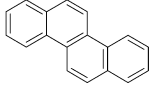
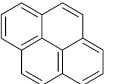
From Table 6 it becomes immediately clear that the new ch-AUA potential significantly improves the accuracy to reproduce the shear viscosities in comparison to the noncharged AUA potential. Considering an uncertainty of about 10% regarding the viscosity prediction and averaging the AAD% values for naphthalene, anthracene, and phenanthrene, the use of the ch-AUA potential leads to viscosities that are in good agreement with experimental values. As it was previously shown for monoaromatic compounds,^{12–14} the noncharged AUA potential seems to systematically underestimate the shear viscosity of naphthalene. This has been attributed to the nonexplicit consideration of the electronic cloud. For anthracene, both AUA and ch-AUA potentials underestimate the shear viscosity, but the AAD is less important in the case of ch-AUA. In the case of phenanthrene both potentials overestimate the viscosity at high temperatures. Nevertheless, the prediction of the viscosity is strongly improved using the ch-AUA potential.

As the new ch-AUA potential improves the prediction of the viscosity, it was then used to compute viscosities of heavier PAH at different temperatures. We have chosen to restrain our study to aromatic polycyclic molecules containing up to four rings, avoiding the small bending that may occur between the rings in long polycyclic aromatics. The molecules studied are fluoranthene, tetracene (benz[β]anthracene), chrysene, and pyrene (Table 7). In the case of fluoranthene, instead of

TABLE 6: Comparison between Experimental Viscosities from the DIPPR Database³⁷ and Shear Viscosities of Naphthalene, Anthracene, and Phenanthrene Obtained by Simulations with the Proposed ch-AUA and the Noncharged AUA Potential

molecule	T (K)	model	η (calcd) (mPa·s)	η (expt) (mPa·s)	% error	model	AAD %
naphthalene	400	AUA	0.546	0.579	-5.71	AUA	16.8
		ch-AUA	0.572		-1.24		
	600	AUA	0.150	0.208	-27.81	ch-AUA	9.1
		ch-AUA	0.173		-16.88		
anthracene	500	AUA	0.615	0.653	-5.78	AUA	17.9
		ch-AUA	0.594		-8.99		
	600	AUA	0.280	0.400	-30.07	ch-AUA	11.3
		ch-AUA	0.346		-13.55		
phenanthrene	450	AUA	1.422	0.788	80.54	AUA	45.7
		ch-AUA	1.049		33.21		
	600	AUA	0.330	0.298	10.84	ch-AUA	18.9
		ch-AUA	0.312		4.68		

TABLE 7: Predicted Shear Viscosities Obtained by Simulations with the Proposed ch-AUA Potential for Fluoranthene, Chrysene, Tetracene (Benz[β]anthracene), and Pyrene Molecules^a

Molecule	T (K)	η calc. (mPa·s)	η corr. (mPa·s)
fluoranthene 	500	1.338	0.985
	700	0.287	0.231
benz[β]anthracene 	700	0.569	0.521
	800	0.210	0.292
chrysene 	600	2.430	0.268
	700	1.006	0.129
pyrene 	500	1.103	0.843
	650	0.416	0.292

^a Correlation data are provided by refs 37 and 42.

considering this molecule as tricyclic with its corresponding point charges, the molecule was thought as the concatenation of one naphthalene and one benzene molecule. Table 7 compares the predicted viscosity values for the studied polycyclic aromatics with data provided by correlation curves.⁴² Except for chrysene, values obtained by simulations are consistent with those provided by the correlation curves. Using the correlation curves^{37,42} at 600 K, the following ranges of viscosity are calculated: (i) for benzene, 0.037–0.052 mPa·s; (ii) for naphthalene, 0.187–0.208 mPa·s; (iii) for anthracene, 0.334–0.400 mPa·s; (iv) and for phenanthrene, 0.294–0.298 mPa·s. Consequently, one can think that the value returned by the correlation curve for chrysene at 600 K (0.268 mPa·s) is too small.

In previous sections the comparison between noncharged AUA and the new ch-AUA potential was realized at different

temperatures. Hereafter, the comparison of the two potentials concerns the evolution of the viscosity of 1-methylnaphthalene at 473.15 K with increasing pressure.

Nieto-Draghi et al. have reproduced experimental values of the dipole moment (μ) of alkylbenzene molecules by shifting by $\delta\mu$ the central positive charge in the plane of the molecule to match the direction and the magnitude of this vector property.^{13,14} Quantum mechanical calculations, as previously detailed, were performed on several monoalkylnaphthalene molecules in order to compute their dipole moments. The average dipole moment was found to be 0.5 D. The equation

$$|\mu| = q \delta\mu \quad (12)$$

where $q = 2q$ (see Figure 3) was used to determine the displacement $\delta\mu$ which corresponds to the distance between the central positive charge and the projections of the negative charges on the plane of the molecule; consequently $\delta\mu = 1.68 \times 10^{-2}$ Å.

Simulation results of 1-methylnaphthalene performed at 473.15 K with the noncharged AUA and ch-AUA potentials are gathered in Table 8 and illustrated in Figure 10, where they are compared with experimental data.⁴³ From these values it appears that the noncharged AUA potential gives results that are in better agreement with experimental data at atmospheric pressure. Taking into account the 10% of uncertainty on the viscosity calculation, the AUA and ch-AUA potentials approach the experimental value. When the pressure increases, the simulations performed with the new ch-AUA potential lead to results that are more consistent with experimental measurements, compared to those obtained with the noncharged AUA potential.

5. Conclusion

In this work, we have proposed a method to compute efficiently thermophysical properties, such as density, vaporization enthalpy, vapor pressure, and viscosity for polycyclic aromatic hydrocarbons, based on an extension of the charged AUA potential that was previously optimized for monoaromatic

TABLE 8: Comparison between Shear Viscosities of 1-Methylnaphthalene Obtained by Simulations with the Proposed ch-AUA and the AUA Potentials and Experimental Data Provided by Ref 43

pressure (MPa)	model	density (kg·m ⁻³)			viscosity (mPa·s)		
		simul	expt	% error	simul	expt	% error
0.1	AUA	904.4	882.8	2.5	0.362	0.364	-0.5
	ch-AUA	908.3		2.9	0.404		10.9
121.6	AUA	998.9	975.5	2.4	1.014	0.802	26.5
	ch-AUA	995.0		2.0	0.958		19.5
200.2	AUA	1034.9	1011.0	2.4	1.738	1.160	49.8
	ch-AUA	1028.6		1.7	1.497		29.1

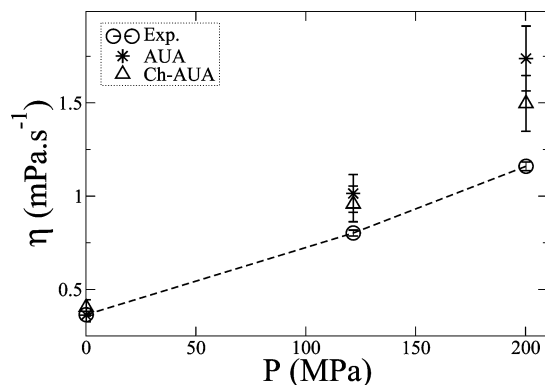


Figure 10. Shear viscosities of 1-methylnaphthalene computed with the proposed ch-AUA and the noncharged AUA potentials and compared with experimental data provided by ref 43.

compounds. This new ch-AUA potential shows a significant gain of computational time compared to traditional all-atoms force field and can be applied to heavy hydrocarbon molecules.

The charged AUA potential uses the same force and mass centers as in noncharged AUA potential, but has been extended with three point charges to mimic the π -clouds of the aromatic molecules. The magnitude of those point charges and the parameters of quaternary carbon bridging two aromatic rings were optimized on the basis of experimental values for naphthalene, leading to the new ch-AUA potential model.

Comparison of the new potential (ch-AUA) to the noncharged AUA (and experimental data) for di- and tricyclic compounds shows that the density, vaporization enthalpy, and vapor pressure, computed at different temperatures, are equally well reproduced with the new ch-AUA potential. Moreover, for the calculations of viscosity at different temperatures, for the naphthalene, anthracene, and phenanthrene molecules, the new ch-AUA potential clearly outperforms the noncharged AUA.

It is also important to remark that the new potential leads to a better general agreement with experimental viscosity data, especially at high temperatures. This coincides with our objective to compute the viscosity of diesel fuels in engines under working conditions (high temperature and pressure). Finally, comparisons between results of simulations performed at high pressures (200 MPa) have shown that the new potential noticeably decreases the relative error, compared to the non-charged AUA potential.

Acknowledgment. The authors would like to thank Bernard Rousseau for the use of the Newton code.

Supporting Information Available: Quadrupolar moments of different PAH computed using DFT quantum mechanical calculations. This material is available free of charge via the Internet at <http://pubs.acs.org>.

References and Notes

- (1) Bansal, V.; Kapur, G. S.; Sarpal, A. S.; Kagdiyal, V.; Jain, S. K.; Srivastava, S. P.; Bhatnagar, A. K. *Energy Fuels* **1998**, *12*, 1223.
- (2) Briker, Y.; Ring, Z.; Iaccchelli, A.; McLean, N.; Rahimi, P. M.; Fairbridge, C. *Energy Fuels* **2001**, *15*, 23.
- (3) Jorgensen, W. L.; Maxwell, D. S.; Tirado-Rives, J. *J. Am. Chem. Soc.* **1996**, *118*, 11225.

- (4) Bourasseau, E.; Ungerer, P.; Boutin, A.; Fuchs, A. H. *Mol. Simul.* **2002**, *28*, 317.
- (5) Bourasseau, E.; Haboudou, M.; Boutin, A.; Fuchs, A. H.; Ungerer, P. *J. Chem. Phys.* **2003**, *118*, 3020.
- (6) Contreras-Camacho, R. O.; Ungerer, P.; Boutin, A.; Mackie, A. D. *J. Phys. Chem. B* **2004**, *108*, 14109.
- (7) Contreras-Camacho, R. O.; Ungerer, P.; Ahunbay, M. G.; Lachet, V.; Perez-Pellitero, J.; Mackie, A. D. *J. Phys. Chem. B* **2004**, *108*, 14115.
- (8) Ahunbay, M. G.; Kranias, S.; Lachet, V.; Ungerer, P. *Fluid Phase Equilib.* **2004**, *224*, 73.
- (9) Ahunbay, M. G.; Perez-Pellitero, J.; Contreras-Camacho, R. O.; Teuler, J. M.; Ungerer, P.; Mackie, A. D.; Lachet, V. *J. Phys. Chem. B* **2005**, *109*, 2970.
- (10) Nieto-Draghi, C.; Ungerer, P.; Rousseau, B. *J. Chem. Phys.* **2006**, *125*, 044517.
- (11) Nieto-Draghi, C.; Bocahut, A.; Creton, B.; Have, P.; Ghoufi, A.; Wender, A.; Boutin, A.; Rousseau, B.; Normand, L. *Mol. Simul.* **2008**, *34*, 211.
- (12) Bonnaud, P.; Nieto-Draghi, C.; Ungerer, P. *J. Phys. Chem. B* **2007**, *111*, 3730.
- (13) Nieto-Draghi, C.; Bonnaud, P.; Ungerer, P. *J. Phys. Chem. C* **2007**, *111*, 15686.
- (14) Nieto-Draghi, C.; Bonnaud, P.; Ungerer, P. *J. Phys. Chem. C* **2007**, *111*, 15942.
- (15) Errington, J. R.; Panagiotopoulos, A. Z. *J. Chem. Phys.* **1999**, *111*, 9731.
- (16) Friedrich, A.; Lustig, R. J. *Mol. Liq.* **2002**, *98*, 241.
- (17) Evans, D. J.; Watts, R. O. *Mol. Phys.* **1976**, *32*, 93.
- (18) Jorgensen, W. L.; Severance, D. L. *J. Am. Chem. Soc.* **1990**, *112*, 4768.
- (19) Jorgensen, W. L.; Laird, E. R.; Nguyen, T. B.; Tirado-Rives, J. *J. Comput. Chem.* **1993**, *14*, 206.
- (20) Wick, C. D.; Martin, M. G.; Siepmann, J. I. *J. Phys. Chem. B* **2000**, *104*, 8008.
- (21) Van-Oanh, N.-T.; Houriez, C.; Rousseau, B. *Phys. Chem. Chem. Phys.* **2010**, *12*, 930.
- (22) Berendsen, H. J. C.; Postma, J. P. M.; Van Gunsteren, W. F.; DiNola, A.; Haak, J. R. *J. Chem. Phys.* **1984**, *81*, 3684.
- (23) Dysthe, D.; Fuchs, A. H.; Rousseau, B. *J. Chem. Phys.* **2000**, *112*, 7581.
- (24) Ungerer, P.; Tavittian, B.; Boutin, A. *Applications of molecular simulation in the oil and gas industry- Monte Carlo methods*; Edition Technip: Paris, 2005.
- (25) Allen, M. P.; Tildesley, D. J. *Computer simulation of liquids*; Oxford Science Publications: Oxford, U.K., 1987.
- (26) Panagiotopoulos, A. Z. *Mol. Phys.* **1987**, *61*, 813.
- (27) Smit, B.; Karaborni, S.; Siepmann, J. I. *J. Chem. Phys.* **1995**, *102*, 2126.
- (28) Bourasseau, E.; Ungerer, P.; Boutin, A. *J. Phys. Chem. B* **2002**, *106*, 5483.
- (29) Ungerer, P.; Beauvais, C.; Delhommelle, J.; Boutin, A.; Rousseau, B.; Fuchs, A. H. *J. Chem. Phys.* **2000**, *112*, 5499.
- (30) *Jaguar*, version 7.0; Schrödinger LLC: New York, NY, 2007.
- (31) Chirlian, L. E.; Francel, M. M. *J. Comput. Chem.* **1987**, *8*, 894.
- (32) Woods, R. J.; Khalil, M.; Pell, W.; Moffat, S. H.; Smith, V. H. *J. Comput. Chem.* **1990**, *11*, 297.
- (33) Breneman, C. M.; Wiberg, K. B. *J. Comput. Chem.* **1990**, *11*, 361.
- (34) Dennis, G. R.; Ritchie, G. L. D. *J. Phys. Chem.* **1991**, *95*, 656.
- (35) Vbrancich, J.; Ritchie, G. L. D. *J. Chem. Soc., Faraday Trans. 2* **1980**, *76*, 648.
- (36) Vbrancich, J.; Ritchie, G. L. D. *Chem. Phys. Lett.* **1983**, *94*, 63.
- (37) Rowley, R. L.; Wilding, W. V.; Oscarson, J. L.; Yang, Y.; Zundel, N. A.; Daubert, T. E.; Danner, R. P. *DIPPR Data Compilation of Pure Compound Properties*; Design Institute for Physical Properties, AIChE: New York, NY, 2003.
- (38) Desgranges, C.; Hicks, J. M.; Magness, A.; Delhommelle, J. *Mol. Phys.* **2010**, *108*, 151.
- (39) Soper, A. K. *Chem. Phys.* **2000**, *258*, 121.
- (40) Soper, A. K. *Mol. Phys.* **2001**, *99*, 1503.
- (41) Laaksonen, A.; Stilbs, P.; Wasylishen, R. *J. Chem. Phys.* **1998**, *108*, 455.
- (42) Yaws, C. L. *Chemical properties handbook: physical, thermodynamic, environmental, transport, safety and health related properties for organic and inorganic chemicals*; McGraw-Hill: New York, 1999.
- (43) Caudwell, D. R.; Trusler, J. P. M.; Vesovic, V.; Wakeham, W. A. *J. Chem. Eng. Data* **2009**, *54*, 359.

JP101649G